Experimental investigation of the heat and fluid flow of an Al2O3-water nanofluid in the laminar-turbulent transition region

Alexandre Briclot, Jean François Henry, Catalin Viorel Popa, Cong Tang Nguyen, Stéphane Fohanno

Version of Record: https://www.sciencedirect.com/science/article/pii/S1290072920309996
Manuscript_360c1d76267656588fece19478a961c4

Experimental investigation of the heat and fluid flow of an Al_2O_3-water nanofluid in the laminar-turbulent transition region

A. Briclot[a], J.F. Henry[a], C. Popa[a,*], C.T. Nguyen[b], S. Fohanno[a]

[a]*ITheMM EA7548, Université de Reims Champagne-Ardenne, Campus Moulin de la Housse, 51100 Reims, France*
[b]*Mechanical Engineering, Université de Moncton, E1A 3E9, NB, Canada*

Abstract

Nanofluids present enhanced thermal conductivity compared to their base fluid and then have become good candidates for heat transfer fluids. In this study, the convective heat transfer coefficient and the pressure drop are measured in a circular tube of inner diameter 4.4 mm and outer diameter 5 mm. The experiments were conducted from Reynolds number Re_D of 500 up to 4500. After making sure that the results for water were in good agreement with the literature, five concentrations of a γ-Al_2O_3-water nanofluid were tested. The results show that the concentration has no impact on the critical Reynolds number corresponding to the laminar-turbulent transition for this nanofluid up to 5w%. Moreover, a slight enhancement of the convective heat transfer coefficient is noted in laminar flow with increasing mass concentration while no significant amelioration is observed in turbulent regime compared to water. On the other hand, the pressure drop strongly increases with concentration whatever the flow regime. As a result, the thermal performance (Convective heat transfer coefficient at constant pumping power) of this nanofluid is lower than pure water.

Keywords: nanofluid, laminar-turbulent transition, heat transfer coefficient, thermal performance

Introduction

Since Maxwell [1], it is known that adding particles into a fluid increases the thermal conductivity of the mixture. With the development of nanotechnologies, side effects of the usage of millimetric and micrometric particles like erosion, sedimentation and an increase in pressure drop have attenuated. Choi and Eastman [2] coined the term nanofluid to describe a nanoparticle-laden fluid. Metallic or ceramic nanoparticles are often used due to their high thermal conductivity compared to base fluids like water or oil. Although many publications exclusively deal with the thermophysical properties of nanofluids [3-11], the results are heterogeneous, especially for the thermal conductivity and the viscosity making the development of a single correlation difficult. Turgut *et al.* [6], Barbés *et al.* [7] and Yang *et al.* [12] measured thermal conductivities of various nanofluids in good agreement with the model of Hamilton-Crosser (HC) [13]. On the other hand, Murshed *et al.* [4] reported increases in thermal conductivity of 18% and 45% for a particle volume concentration of 5% of Al and TiO_2 in ethylene glycol which is much higher than the predicted values of HC model. They proposed a model to determine the relative thermal conductivity taking into account the particle size and the thickness

*Corresponding author
Email address: catalin.popa@univ-reims.fr (C. Popa)

Nomenclature

Symbols

$\dot{m}$	Mass flow rate
C_p	Specific heat
d	Diameter
e	Thickness
h	Convective heat transfer coefficient
I	Intensity
K	Instrument constant
k	Thermal conductivity
L	Pipe length
Nu	Nusselt number
Pr	Prandtl number
$q"$	Heat flux
Ra	Rayleigh number
Re_D	Reynolds number
S	Surface
T	Temperature
t	Time
U	Voltage
V	Velocity
x	Axial coordinate
v%	Volume fraction
w%	Mass fraction

Greek Letters

ΔP	Pressure drop
γ	Kinematic energy correction
λ	Friction factor
μ	Dynamic viscosity
ν	Kinematic viscosity
ϕ_m	Mass concentration
ϕ_v	Volume concentration
ρ	Density, resistivity
σ	Stefan-Boltzman constant
ε	Emissivity

Subscripts

a	Ambient
BF	Base fluid
c	Convective
e	External
i	Internal
in	Inlet
NF	Nanofluid
NP	Nanoparticles
p	Pressure
r	Relative, radiative

Superscripts

+	Dimensionless

of a nanolayer at the nanoparticle-fluid interface.

Besides the positive effect of the nanoparticle on the thermal conductivity, their presence also increases the viscosity of the mixture. For very dilute suspensions, Einstein [14] developed a theoretical model depending on the volume concentration only to predict the increase in viscosity. Later, Brinkman [15] and Batchelor [16] extended Einstein's model to higher concentrations. However, even at very low volume concentrations ($\varphi_v < 1\%$), these three models often fail to predict correctly the evolution of viscosity for Al_2O_3-water [5, 10, 12, 17-19] and TiO_2-water [6, 17] nanofluids. The discrepancies between the theoretical predictions and the experimental results can be attributed to the numerous parameters to take into account in the determination of the thermophysical properties of nanofluids, like the size of the nanoparticles, their shapes, the pH of the solution etc. As the theoretical models often fail to predict the change in the properties of nanofluids, several empirical correlations are available in the literature and compiled by Khanafer and Vafai [20].

Due to their enhanced thermal conductivity, nanofluids have become good candidates for heat transfer

fluids. Kim *et al.* [21] studied the flow of an Al_2O_3-water nanofluid in a pipe and reported an enhancement of 15% and 20% in the convective heat transfer coefficient in laminar and turbulent regimes respectively. At 0.3 v% of Al_2O_3 in water, Hwang *et al.* [19] observed an increase of 8% in the convective heat transfer coefficient in laminar flow that is higher than the enhancement of the thermal conductivity (+1.44%). The friction factor is unchanged with the increasing volume concentration up to 0.3% while the viscosity is 3% higher than pure water at the maximum volume concentration. Wen and Ding [22] showed that the thermal entrance length of nanofluids is greater than that of pure fluid in laminar flow. They suggested that the particle migration due to high velocity gradient in the entrance length could affect the development of the boundary layer and then can be responsible for the anomalous heat transfer enhancement. However, the increase in pressure drop is not always considered while it is an important feature of a heat exchanger. Pak and Cho [17] already noted in 1998 that under the condition of constant velocity, the convective heat transfer coefficient is higher for water than for nanofluids because of the high increase in viscosity. This observation is confirmed by other studies [23-26] constituting a potential hindrance for the usage of nanofluids in industrial applications where the pumping power is important.

To our knowledge, only a few studies deal with the laminar-turbulent transition. Liu and Yu [27], Meyer *et al.* [28] and Nikulin *et al.* [29] studied the convective heat transfer and the pressure drop of a flow of a nanofluid in the laminar-turbulent transition region while Rudyak *et al.* [30] investigated the laminar-turbulent transition ($1000 \leq Re_D \leq 9000$) through the friction factor only. In [27], it has been shown that the presence of the nanoparticles of Al_2O_3 (40 nm nominal diameter) in water shifts the transition to higher Reynolds numbers in pipe flows and that nanofluids should be used in laminar or fully turbulent flows with sufficiently high Reynolds number to present an interest in cooling applications. On the other hand, in [28], [29] and [30], the authors noted that the laminar-turbulent transition occurred earlier for nanofluids of MWCNT-water (d_{NP} = 20 nm×20 µm), Al_2O_3-isopropanol (d_{NP} = 8 nm as dry powder and 80 nm in solution) and SiO_2-water (25 nm and 100 nm nominal diameter) respectively compared to base fluids alone.

In this study, we conducted an experimental investigation of the convective heat transfer coefficient h and the linear pressure drop ΔP of a nanofluid (10 nm γ-Al_2O_3 in deionized (DI) water) in a pipe flow for several mass concentrations ($0.75\% \leq \phi_m \leq 5\%$) and Reynolds numbers from 500 up to 4500. The objectives of this work are to study the flow and heat transfer of this nanofluid in the laminar-turbulent region and to determine its thermal performance compared to that of water based on the recommendation of Yu *et al.* [31].

1. Nanofluid characterisation

The nanofluids used in this work are suspended γ-Al_2O_3 nanoparticles of 10 nm mean diameter, dispersed in DI water without any surfactant. The stock solution is a 20w% solution supplied by the manufacturer Nanostructured & Anamorphous Materials, Inc. DI water is used to dilute the stock solution and to obtain mass concentrations of 0.75%, 1.5%, 2.5%, 3.5% and 5%.

The density and specific heat capacity of these nanofluids are determined by mixtures laws:

$$\rho_{NF} = \phi_v \rho_{NP} + (1 - \phi_v)\rho_{BF}, \quad (1)$$

$$\rho_{NF} C_{p,NF} = \phi_v \rho_{NP} C_{p,NP} + (1 - \phi_v)\rho_{BF} C_{p,BF}. \quad (2)$$

The density and the specific heat capacity of Al_2O_3 nanoparticles are respectively 3700 kg·m^{-3} and 773

$J \cdot kg^{-1} \cdot K^{-1}$. The volume concentration is determined from the mass concentration and the densities of the base fluid and the nanoparticles:

$$\phi_v = \frac{\phi_m}{\phi_m + \left(\frac{\rho_{NP}}{\rho_{BF}}\right)(1 - \phi_m)}. \tag{3}$$

The work of Minakov et al. [32] suggests that the Al_2O_3-water nanofluids are Newtonian up to 2v%. In the present study, the Newtonian behaviour has been verified with a rheometer Rheomat RM100 (Lamy Rheology) in the range of the studied concentrations. Therefore, the kinematic viscosity of our nanofluids ν has been measured with an Ubbelohde viscometer from 15°C to 30°C. The determination of the kinematic viscosity is based on the flow time t of the fluid through a capillary tube of 0.47 mm diameter:

$$\nu = K(t - \gamma), \tag{4}$$

where K and γ are respectively the instrument constant and the kinematic energy correction. To avoid any human error in the process, the flow time is automatically measured by a ViscoClock *plus* module from SI analytics. The experiment is repeated three times for each configuration and the present results are the arithmetic means.

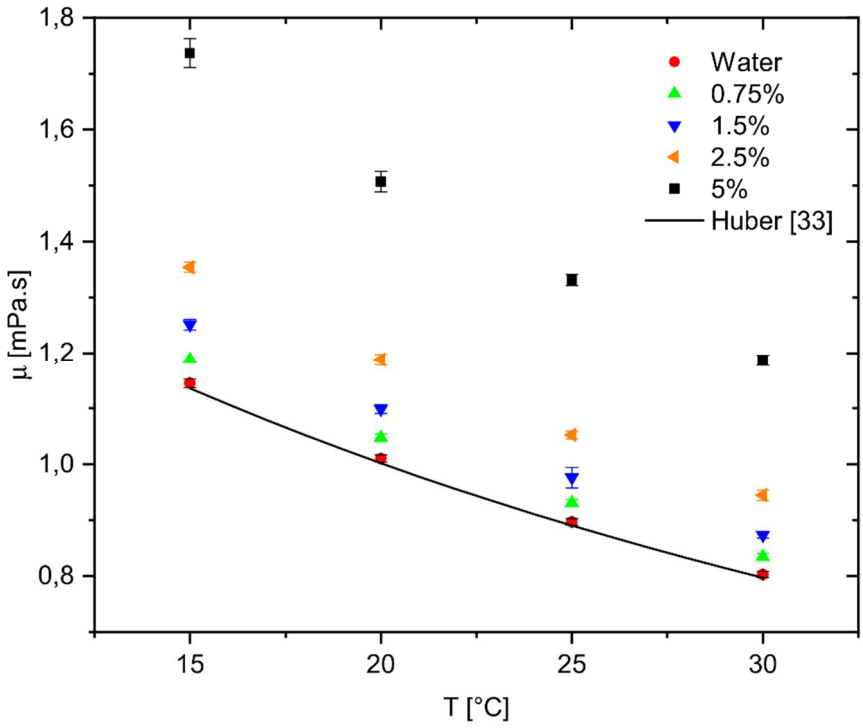

Figure 1: Dynamic viscosity versus temperature for different concentrations of nanofluid.

Figure 1 presents the dynamic viscosity (obtained by multiplying the kinematic viscosity with the density determined by Eq. (1)) as a function the temperature. The measured viscosity of water is in very good accordance with the literature [33] as the maximum relative deviation is 0.84%. The viscosity of the nanofluid clearly increases with mass concentration and its evolution as a function of the temperature follows the same trend as water. Actually, the relative viscosity $\mu_r = \mu_{NF}/\mu_{BF}$ is

independent of the temperature and can be described by the following equation:

$$\mu_r = 1 + 16.54\phi_v + 1329\phi_v^2 \tag{5}$$

Consequently, the properties of nanofluids are estimated at the mean temperature of the flow in the test section, their temperature dependence being implicitly taken into account through the base fluid properties.

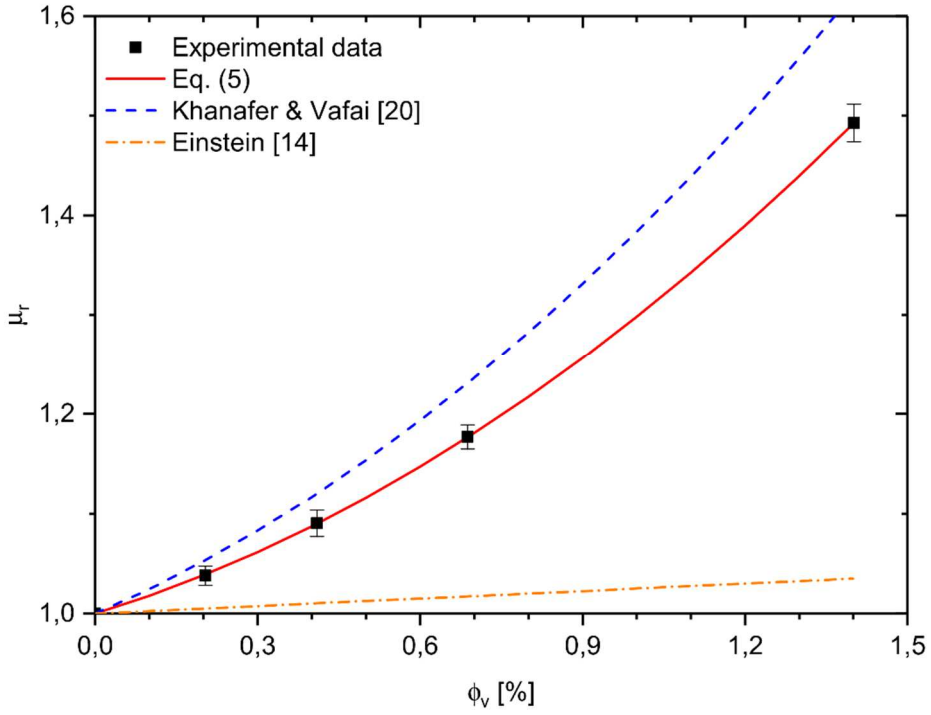

Figure 2: Relative viscosity versus volume fraction.

Figure 2 compares the experimental results with Eq. (5) and two models from the literature [14, 20]. It can be seen that the theoretical model of Einstein [14] is not appropriated for this nanofluid while the correlation of Khanafer and Vafai [20] obtained from curve-fitting the measurements of Pak and Cho [17] (Al_2O_3-water nanofluid, d_{NP} = 13 nm) overestimates the present results. This discrepancy can be due to the difference of pH allowing a better dispersion of the nanoparticles in [17], decreasing their effective diameter.

2. Experimental set-up

The flow loop is composed of a gear pump, a temperature controlled water bath, a 1.56 m long straight copper tube with inner diameter d_i = 4.4 mm and outer diameter d_e = 5.0 mm, an ultrasonic bath and a flowmeter (Figure 3). The copper tube is electrically heated by Joule heating on 41.4 cm after a 1 m entry length to avoid entry effect ($L/d_i \approx 220$). It is covered with a matte black paint with an emissivity ε of 0.93±0.01 that allows the recording of the external wall temperature thanks to a thermal camera (CEDIP-FLIR Titanium, 640×512 pixels, Spectral range from 1.5 to 5.1 µm, NETD 20 mK at 20°C). The measurement area represents 6×2.4 mm^2. Voltage is directly recorded by a GRAPHTEC data logger while intensity is measured by a DC clamp meter. Likewise, volume flow rate and pressure losses are respectively measured by a MACNAUGHT MX06P flowmeter (0.5 to 100 $L{\cdot}h^{-1}$ with ± 0.5% accuracy)

and a KELLER PD23 pressure transmitter with a measuring range of 0.5 bar, both connected to the data logger.

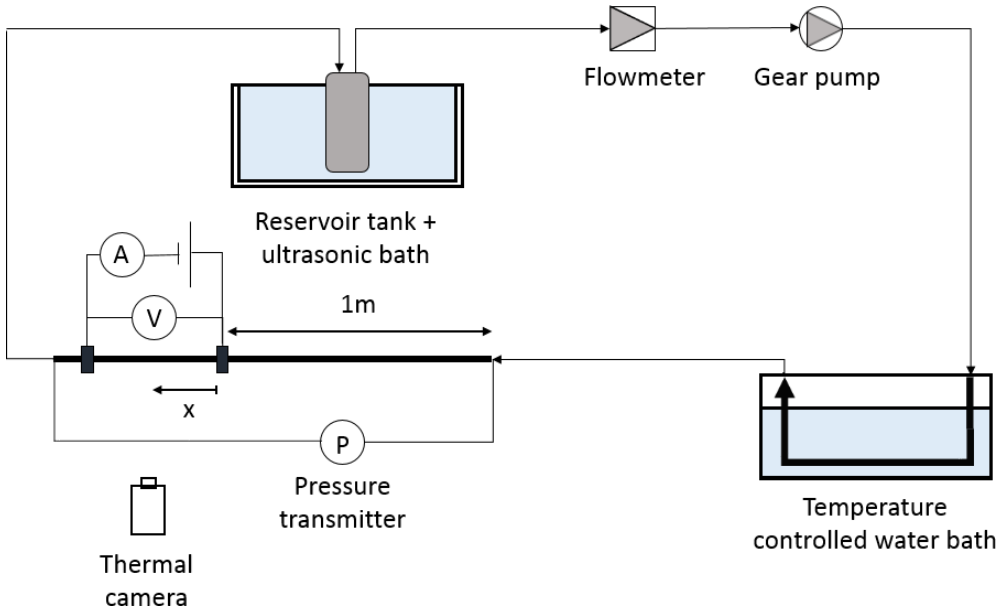

Figure 1: Schematic diagram of the experimental set-up.

The convective heat transfer coefficient is determined from a thermal balance on the copper tube after an electrical excitation increasing the external wall temperature by 3°C. Once the system has reached the steady state, the recording of the thermograms starts for 40 seconds at a frequency of 5 Hz. After 16 seconds, voltage U and intensity I are cut and the external wall temperature decreases to reach the temperature of the fluid at the inlet of the test zone (Figure 4). This methodology was previously validated for periodic excitations [34] while a Heaviside step function is used here. Moreover, it does not require thermocouples, thus avoiding flow disturbances. Due to the very small thickness of the tube (e = 0.3 mm) and the high thermal conductivity of copper (k = 400 W·m^{-1}·K^{-1}), the internal and external wall temperatures are considered to be equal. Indeed, the maximum power Q used in this study of 70 W (12.2 kW·m^{-2}) would result in a temperature difference ΔT of 9×10^{-3}K between the internal and external walls according to the following equation:

$$\Delta T = Q \frac{\ln(d_e/d_i)}{2\pi L k}. \tag{6}$$

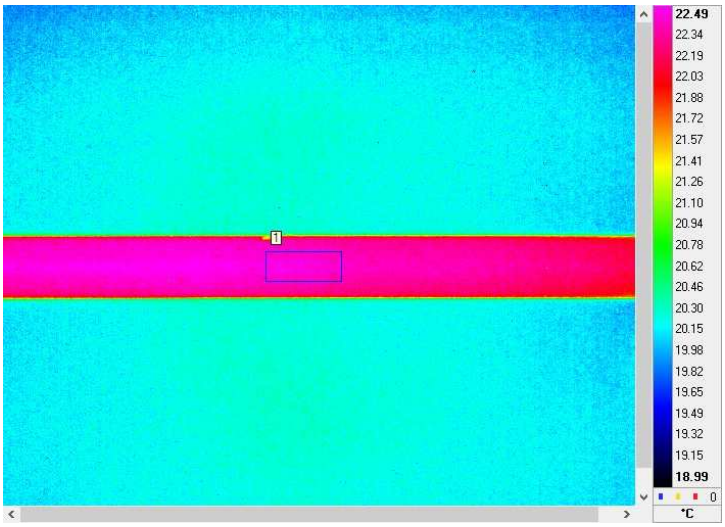

(a)

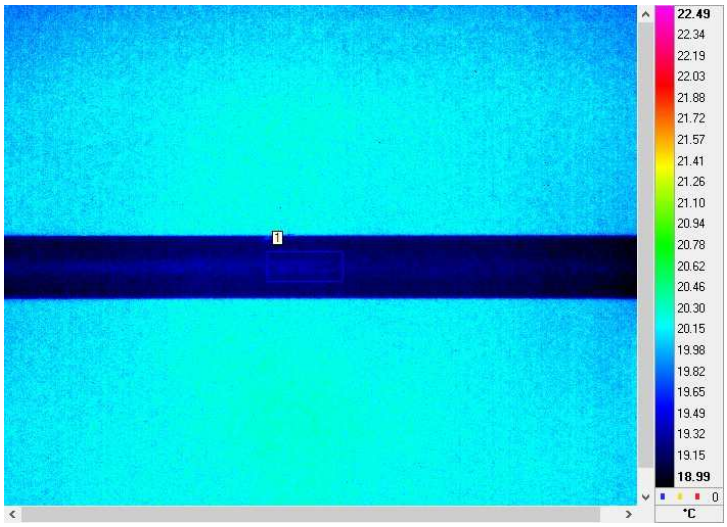

(b)

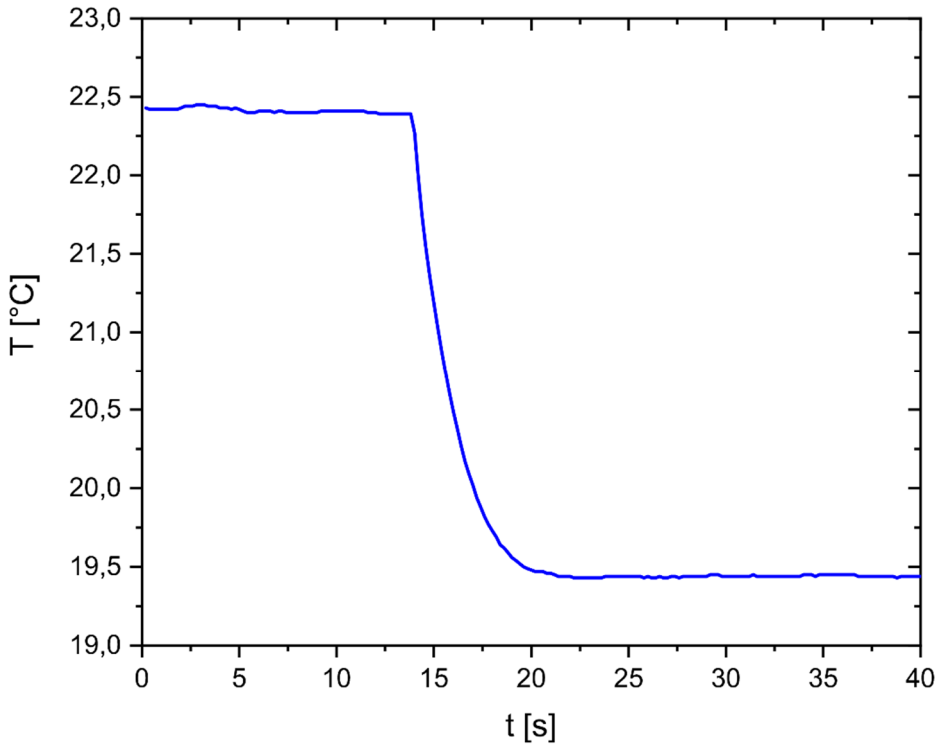

(c)

Figure 4: Thermograms of the copper tube during heating (4a) and at rest (4b) and temperature profile (4c). The measurement area represents 6 × 2.4 mm²

Moreover, the heat losses to the surroundings are estimated. The radiative heat transfer coefficient is obtained by linearizing Stefan-Boltzman law:

$$h_r = \varepsilon\sigma(T_e + T_a)^2(T_e + T_a) \tag{7}$$

where σ, Te and Ta denote the Stefan-Boltzmann constant (5.67 × 10−8 W·m−2·K−4), the external wall temperature and the temperature of surroundings.

The convective heat transfer coefficient to the ambient air is determined with the following equation for horizontal cylinders with a uniform heat flux density [35]:

$$h_c = 0.579\frac{k_a}{d_e}Ra^{1/4}\left[1 + \left(\frac{0.442}{Pr}\right)^{\frac{9}{16}}\right]^{-4/9}, \tag{8}$$

where k_a, Ra and Pr are the thermal conductivity of the air, the Rayleigh number and the Prandtl number respectively.

The global heat transfer coefficient to the surroundings h_e is the sum of h_r and h_c and is about 10 $W{\cdot}m^{-2}{\cdot}K^{-1}$. As a result, the heat losses account for 1% of the heat transferred to the fluid.

The heat flux, generated by Joule heating writes as:

$$q" = \frac{RI^2}{\pi d_i L} = \frac{\rho I^2}{\pi^2 d_i\left(d_e^2 - d_i^2\right)}, \tag{9}$$

where R and ρ respectively denote the electrical resistance and resistivity of the copper tube. As the input current and the electrical resistivity are constant, the heat flux is also constant.

Finally, the energy balance writes as:

$$q" = \frac{UI}{\pi d_i L} = h_i(x)\left(T_e(x) - T_{NF}(x)\right) + h_e\frac{d_e}{d_i}(T_e(x) - T_a), \tag{10}$$

where $T_{NF}(x)$ denotes the temperature of the nanofluid at the x location.

As the heat flux is constant, the local temperature of the fluid follows a linear profile:

$$T_{NF}(x) = T_{NF,in} + \frac{UI\frac{x}{L}}{\dot{m}C_p}, \tag{11}$$

where $\dot{m}$ is the mass flow rate.

Combining equations (10) and (11), the convective heat transfer coefficient writes as:

$$h_i(x) = \frac{UI - h_e S_e(T_e(x) - T_a)}{\pi d_i L\left(T_e(x) - T_{NF,in} - \frac{UI\frac{x}{L}}{\dot{m}C_p}\right)}. \tag{12}$$

The absolute uncertainties are evaluated as described in Appendix A. Measurement uncertainties and the relative uncertainties are listed in Table 1. The relative uncertainties of the pumping power PP, the pressure drop ΔP and the friction factor λ are high at low Reynolds number and quickly decrease. This is due to the accuracy of the pressure transmitter that is a percentage of the full scale.

Table 1: Relative uncertainties

Quantity	Relative uncertainty [%]
Re_D	0.5 – 3.5
PP	3 – 58
ΔP	2.6 – 47
λ	2.9 – 48
$h_i(x)$	3.4 – 6.9

3. Validation case

In order to assess the accuracy of the present results, experiments were first conducted with deionized water as a function of the Reynolds number:

$$Re_D = \frac{\rho V d_i}{\mu}. \tag{13}$$

As the temperature difference between the inlet and the outlet of the test section (eq. 11) is less than 2°C, the thermal properties of the fluid are considered constant and the measured pressure drop is then compared with the Darcy-Weisbasch equation:

$$\Delta P = \lambda \frac{\rho V^2}{2} \frac{L_p}{d_i}, \tag{14}$$

where the friction factor is determined by the well-known Poiseuille's law in laminar flow:

$$\lambda = \frac{64}{Re_D}, \tag{15}$$

In turbulent flow, the correlation of Filonenko [36] is used :

$$\lambda = [1.82 \log(Re_D) - 1.64]^{-2}. \tag{16}$$

According to the flow regime maps developed by Everts and Meyer [37], the flow is forced convection for all Reynolds numbers. Therefore, the convective heat transfer coefficient is compared with the theoretical solution given by Kays and Crawford [38] for forced convection flows in laminar regime accounting for the thermal entrance length effect:

$$Nu_x = \left[\frac{11}{48} - \frac{1}{2} \sum_{m=1}^{\infty} \frac{\exp(-\gamma_m^2 x^+)}{A_m \gamma_m^4} \right]^{-1}, \tag{17}$$

where the eigenvalues and constants are given in [38] and $x^+ = \frac{2x/d_i}{Re_D\, Pr}$.

In turbulent regime, the present results are confronted with the recent correlation of Meyer *et al.* [39]:

$$Nu = 0.0018 {Re_D}^{-0.25} (Re_D - 500)^{1.07} Pr^{0.42} \left(\frac{Pr}{Pr_w} \right)^{0.11}. \tag{18}$$

Figure 5 shows the evolution of the pressure drop for water as a function of the Reynolds number. The experimental measurements are in good agreement with the theoretical results obtained from equations 15 and 16 as the theoretical results are within the error ranges of the data points in laminar and turbulent flows, which confirms the good accuracy and reliability of the experiments.

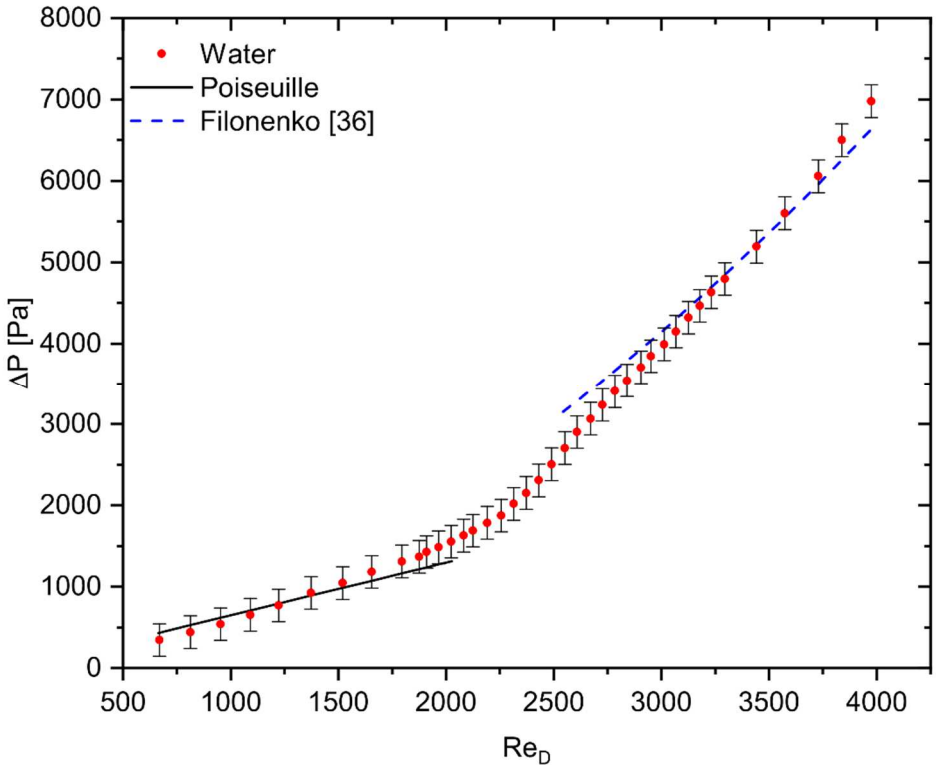

Figure 5: Pressure drop in the test section versus Reynolds number for water.

Similarly, Figure 6 compares the present results of the convective heat transfer coefficient with equations 17 and 18 as a function of the Reynolds number. In laminar regime, the convective heat transfer coefficient increases with the Reynolds number, confirming that the flow is not thermally developed. Moreover, one can observe that our experimental measurements are in very good agreement with the theoretical results in both laminar and turbulent regimes.

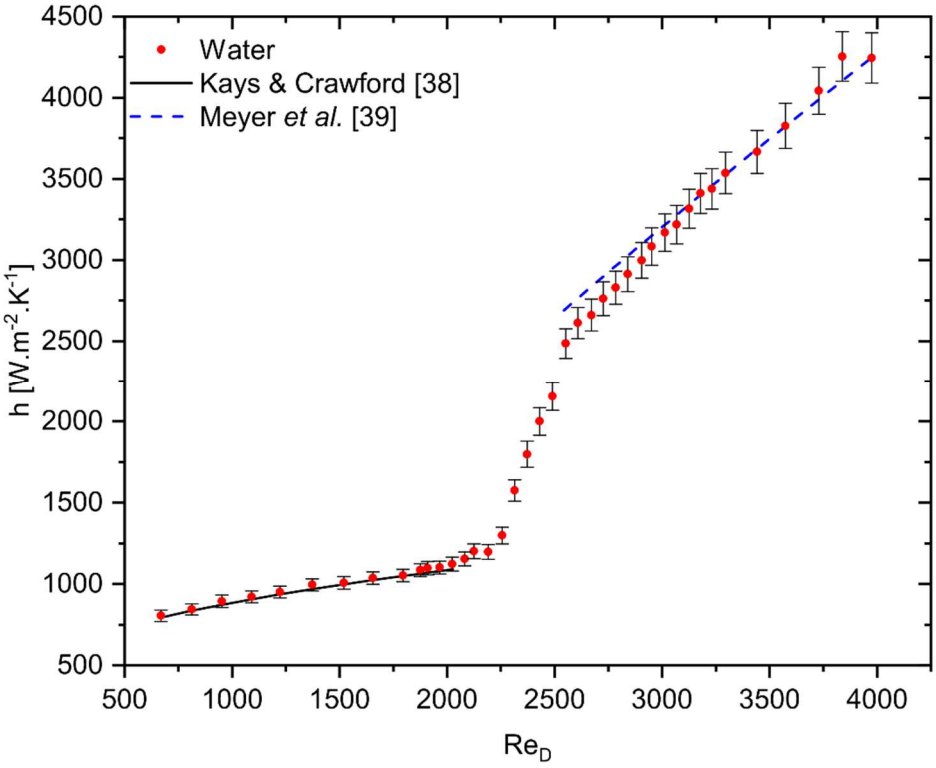

Figure 6: Convective heat transfer coefficient versus Reynolds number for water.

4. Results and discussion

4.1. Convective heat transfer coefficient

Figure 7 presents the evolution of the convective heat transfer coefficient as a function of the Reynolds number for three mass concentrations and water. Low concentrations of nanofluids are not shown to improve readability. In the laminar region (Fig. 7b), the convective heat transfer coefficient increases with mass concentration to reach a 9% enhancement at 5w% compared to water. This enhancement can be due to the increased thermal conductivity or the increased entrance length due to the presence of the nanoparticles [22, 40]. In the entrance region, the thermal boundary layer is thin favoring heat transfer.

On the other hand, in turbulent flow up to Reynolds number of 4000, all the curves collapse together indicating that the nanoparticles do not impact the heat transfer (Fig. 7a). This indicates that the increase in convective heat transfer coefficient observed in laminar regime is not solely due to the increased thermal conductivity, otherwise h_i would be greater in turbulent flow too. However, this is consistent with the hypothesis of a longer entrance length due to the presence of the nanoparticles. Indeed, the thermal entrance length in turbulent flows is short ($\frac{x}{d_i} \approx 10$) while it can become very long in laminar flows $\left(\frac{x}{d_i} \approx 0.05 Re_D Pr\right)$ [41]. As a result, the entrance region is not sufficiently lengthened in turbulent flow to have an impact on the heat transfer.

Furthermore, the mass concentration of this nanofluid has no impact on the onset of the laminar-turbulent transition. Indeed, the critical Reynolds number for the onset of the transition is 2300 ± 50 for all tested fluids and the one for the establishment of fully turbulent flow is around 2600 ± 50. This suggests that this nanofluid behaves like a single-phase fluid with modified properties. This

observation contrasts with the work of Liu and Yu [27] on an Al_2O_3-water nanofluid where the transition is retarded and the studies of Meyer et al. [28] on a MWCNT-water nanofluid, Rudyak et al. [30] on a SiO_2-water nanofluid and Nikulin et al. [29] on an Al_2O_3-isopropanol nanofluid where the transition is accelerated. This discrepancy is potentially due to the difference in the nominal diameter of the nanoparticles in the studies affecting the viscosity of the nanofluid and then the Reynolds number.

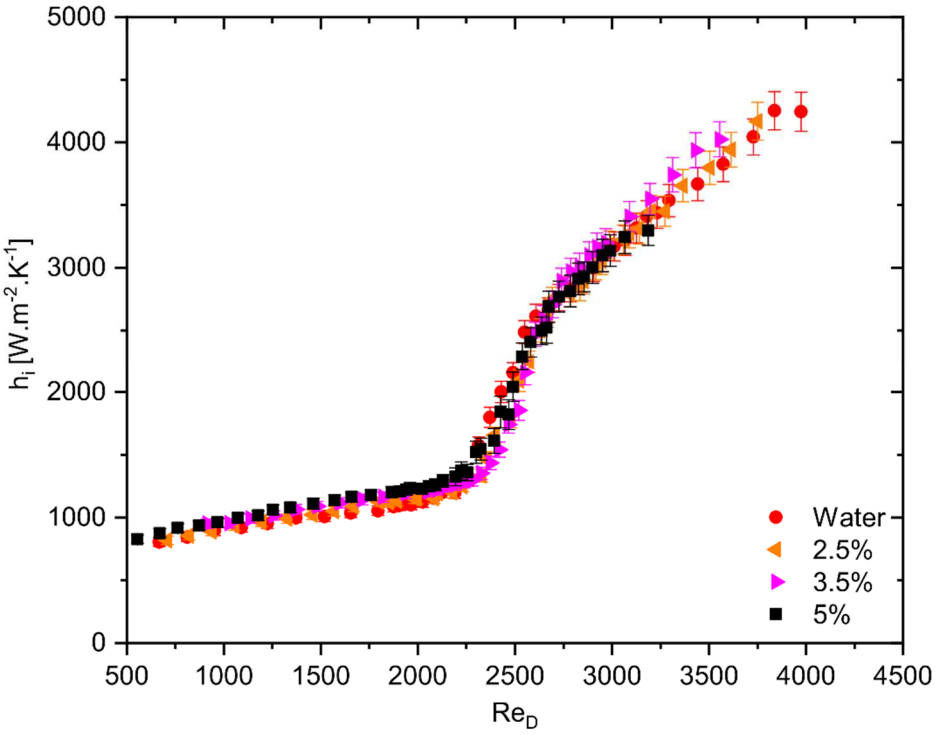

(a)

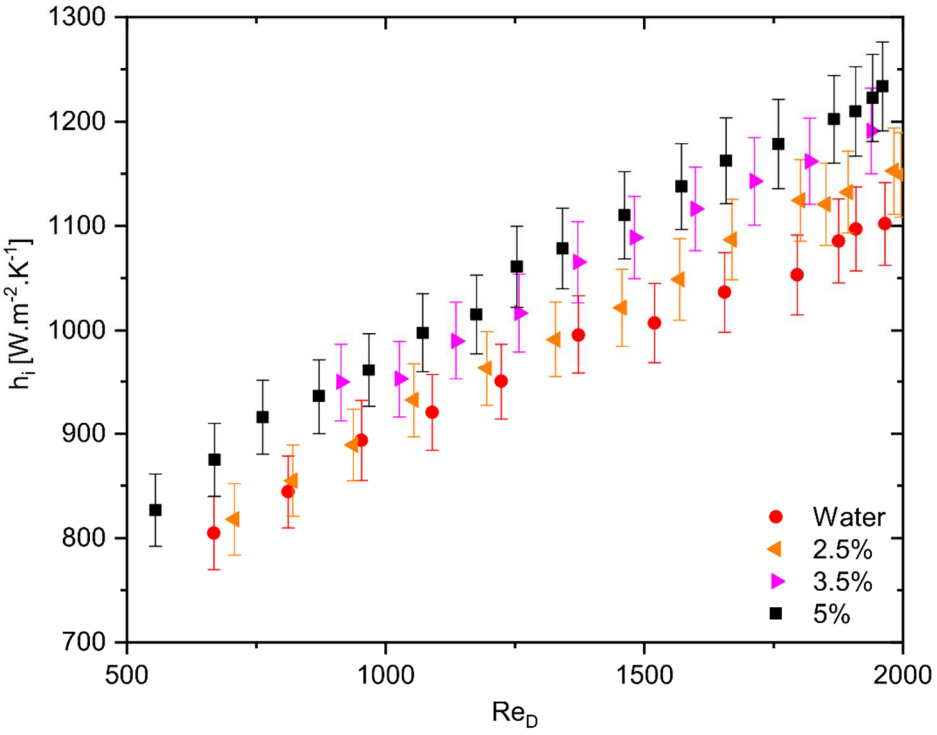

(b)

Figure 7: Convective heat transfer coefficient versus Reynolds number for water and different concentrations of Al_2O_3-water nanofluid (a) with a zoom on the laminar region (b).

4.2. Pressure drop

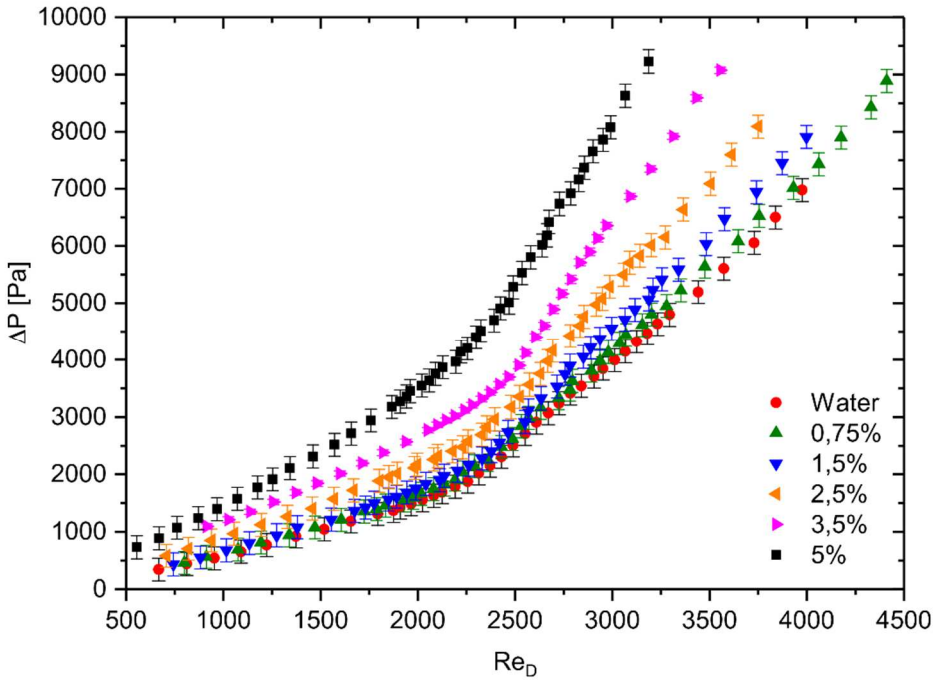

Figure 8: Pressure drop in the test section versus Reynolds number for water and different concentrations of Al_2O_3-water nanofluid.

Figure 8 shows the pressure drop in the test section as a function of the Reynolds number. One can note that the pressure drop significantly increases with the mass concentration whatever the flow regime so that at 5w%, it is more than doubled compared to that of water. Even at a very low mass concentration of 0.75%, the observed increase in pressure drop reaches 7%, which is much higher than the intensification of the convective heat transfer coefficient. The increase in pressure drop is due to the higher viscosity of the nanofluid compared to that of water creating more friction losses at the pipe wall. As the volumetric flow rate and the pressure drop of this nanofluid are higher than these of water, a greater pumping power is required to reach the same Reynolds number. This means that it can be difficult to obtain a fully turbulent flow with high concentrations of nanofluids.

Figure 9 depicts the evolution of the friction factor as a function of the Reynolds number in laminar flow. The data points for the different concentrations of nanofluid are close to those of water. Moreover, they are in relatively good agreement with the theoretical law (eq. 15) up to a Reynolds number of 1500, confirming that the behaviour of this nanofluid is close to that of single-phase fluids. The error bars are bigger at low Reynolds numbers because the uncertainty of the pressure drop is a percentage of the full scale.

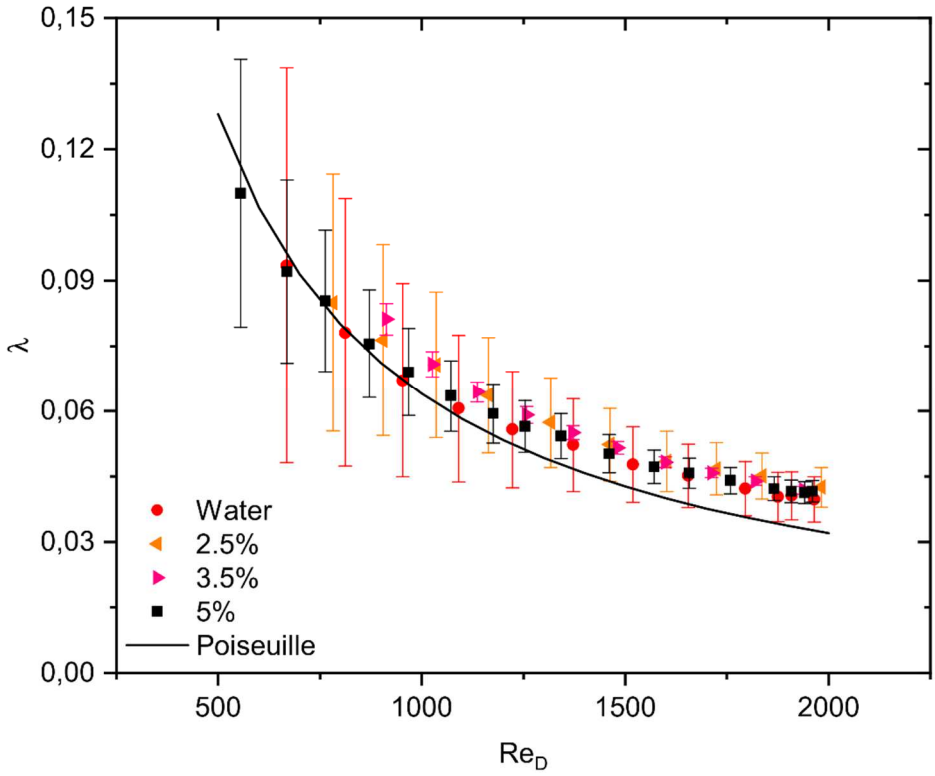

Figure 9: Friction factor versus Reynolds number for water and different concentrations of Al2O3-water nanofluid in laminar regime.

4.3. Figure of merit

To determine the performance of this nanofluid over the base fluid, several figures of merit (FOM) can be used but different conclusions can be drawn. To analyse the performance of heat transfer fluids, it is natural to compare heat transfer coefficients. However, the simple base of constant Reynolds number can lead to inappropriate conclusions. Indeed, for a constant Reynolds number, the mean velocity of the nanofluid would be higher than that of pure water due to the increased viscosity. This would means that the convective heat transfer coefficient increases with viscosity because of the velocity effect. To compare fluids unambiguously, Yu *et al.* [42] recommend to compare the convective heat transfer coefficient in a constant pumping power (PP) basis. Figure 10 depicts the evolution of the heat transfer coefficient as a function of the pumping power necessary to drive the nanofluid in the test section, corresponding to the product of the volumetric flow rate by the pressure drop. In laminar flow (Fig. 10b), low concentrations of nanofluid (0.75w% and 1.5w%) show no significant difference compared to water while higher concentrations clearly deteriorate the thermal performance. Moreover, as the transition occurs at a lower velocity for water (Fig. 10a), a better heat transfer coefficient is reached for the same pumping power. In turbulent flow, the thermal performance decreases with increasing concentration. This nanofluid could still be used in laminar regime at low particle concentrations in applications where the pumping power is not of great concern.

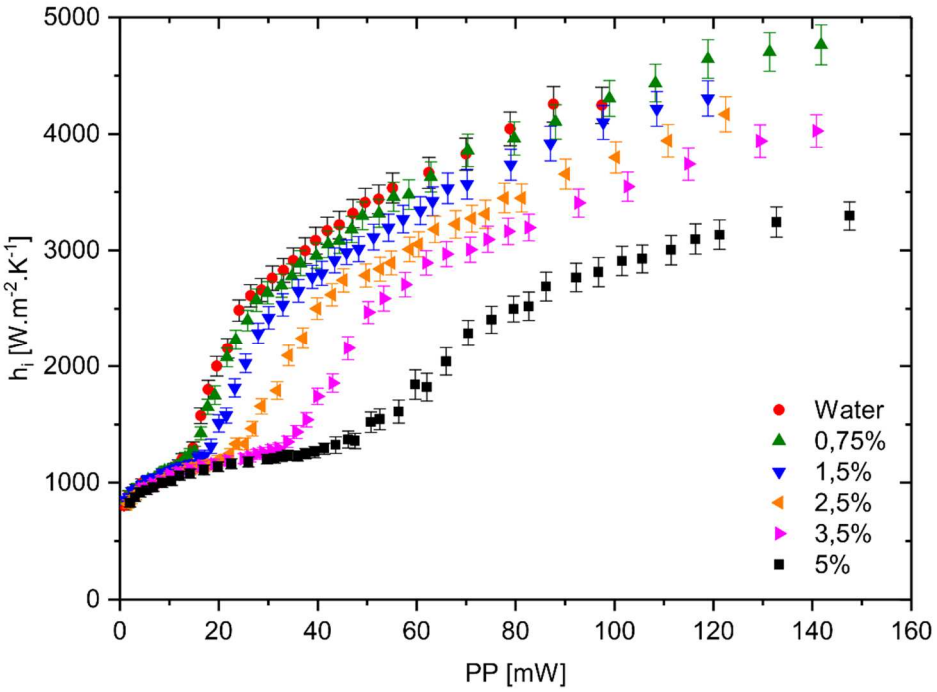

(a)

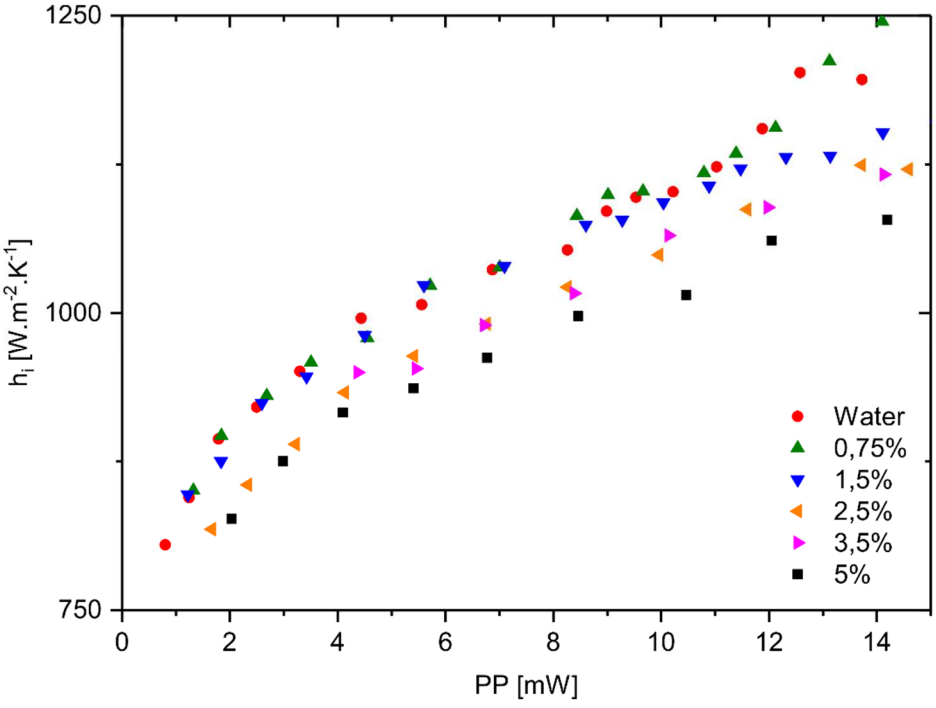

(b)

Figure 10: Convective heat transfer coefficient versus pumping power for water and different concentrations of Al2O3-water nanofluid (a) with a zoom on the laminar region (b).

Conclusion

Convective flows of nanofluids in the transitional region have received little attention in the previous works. Motivated by this fact, experiments were conducted to determine the heat transfer coefficient and the pressure drop in transitional flow through a circular tube with constant heat flux boundary. The accuracy of the present set-up has been successfully verified through a series of experiments with deionized water. Indeed, the theoretical results are included in the range of the experimental error bars for both ΔP and h_i. As a result, five concentrations of an Al_2O_3-water nanofluid have been studied. It has been shown that the presence of the nanoparticle does not affect the onset of the laminar-turbulent transition for this nanofluid up to 5w%, as the critical Reynolds number is around 2300 ± 50 for all tested fluids. Therefore, it suggests that this nanofluid behaves like a single-phase fluid in this range. This assumption is strengthened by the good agreement between the experimental results for the friction factor and the theoretical relationship in laminar flow. However, the increase in pressure drop compared to water exceeds the enhancement of the convective heat transfer coefficient so that the thermal performance is lowered when these nanoparticles are added to water whatever the flow regime. To overcome this problem, one could use nanoparticles with better thermal properties than Al_2O_3 like pure metals. Another possible solution would be to reduce the viscosity of the nanofluids using larger nanoparticles.

Appendix A. Measurement uncertainties

When a quantity X is recorded, (U, I, ΔP, Q_v, T_e, and $T_{NF,in}$), the best estimate is the arithmetic mean of the n measurements [43]:

$$\bar{X} = \frac{1}{n}\sum_{i=1}^{n} X_i. \tag{A.1}$$

The associated type A uncertainty δX_A caused by random fluctuations of the measurements with a 95%-confidence interval is determined by [43]:

$$\delta X_A = t_{95\%,n-1}\frac{\sigma(X)}{\sqrt{n}}, \tag{A.2}$$

where $t_{95\%,n-1}$ is the value of the Student t-distribution with $n-1$ degrees of freedom at 95% confidence and $\sigma(X)$ is the standard deviation defined by :

$$\sigma(X) = \sqrt{\frac{1}{n-1}\sum_{i=1}^{n}(X_i - \bar{X})^2}. \tag{A.3}$$

When a quantity q is derived from N possibly correlated input quantities X_i, i.e. $q = f(X_1, X_2, ..., X_N)$, the combined type A uncertainty of q is :

$$\delta^2 q_A = \sum_{i=1}^{N}\left(\frac{\partial f}{\partial X_i}\right)^2 \delta^2 X_{i,A} + 2\sum_{i=1}^{N-1}\sum_{j=i+1}^{N}\frac{\partial f}{\partial X_i}\frac{\partial f}{\partial X_j}\delta X_{i,A}\delta X_{j,A}\, r_{i,j}, \tag{A.4}$$

with $r_{i,j}$ the correlation coefficient :

$$r_{i,j} = \frac{\sigma(X_i, X_j)}{\sigma(X_i)\sigma(X_j)}. \tag{A.5}$$

where $\sigma(X_i, X_j)$ is the covariance between X_i and X_j.
On the other hand, type B uncertainty calculations due to systematic errors are based on manufacturers' specifications when available. Finally, type A and type B uncertainties are combined to obtain the overall uncertainty of q [43]:

$$\delta^2 q = \delta^2 q_A + \delta^2 q_B. \tag{A.6}$$

Acknowledgements

The authors are grateful to Didier Caron for his technical support. They also thank Maryline Parmentier for sharing with them the viscometer.

References

[1] J. C. Maxwell. *A treatise on electricity and magnetism*. Oxford : Clarendon Press, 1873.

[2] S. U. S. Choi and J. A. Eastman. Enhancing Thermal Conductivity of Fluids With Nanoparticles. *ASME International Mechanical Engineering Congress & Exposition*, pages 99-106, 1995.

[3] R. Mondragón, C. Segarra, R. Martínez-Cuenca, J. E. Juliá, and J. C. Jarque. Experimental characterization and modeling of thermophysical properties of nanofluids at high temperature conditions for heat transfer applications. *Powder Technology*, 249:516-529, 2013.

[4] S. M.S. Murshed, K. C. Leong, and C. Yang. Investigations of thermal conductivity and viscosity of nanofluids. *International Journal of Thermal Sciences*, 47(5):560-568, 2008.

[5] Y. Raja Sekhar and K. V. Sharma. Study of viscosity and specific heat capacity characteristics of water-based Al_2O_3 nanofluids at low particle concentrations. *Journal of Experimental Nanoscience*, 10(2):86-102, 2015.

[6] A. Turgut, I. Tavman, M. Chirtoc, H. P. Schuchmann, C. Sauter, and S. Tavman. Thermal conductivity and viscosity measurements of water-based TiO_2 nanofluids. *International Journal of Thermophysics*, 30(4):1213-1226, 2009.

[7] B. Barbés, R. Páramo, E. Blanco, and C. Casanova. Thermal conductivity and specific heat capacity measurements of CuO nanofluids. *Journal of Thermal Analysis and Calorimetry*, 115(2):1883-1891, 2014.

[8] C.V. Popa, C.T. Nguyen, and I. Gherasim. New specific heat data for Al_2O_3 and CuO nanoparticles in suspension in water and Ethylene Glycol. *International Journal of Thermal Sciences*, 111:108- 115, 2017.

[9] M. A. Hachey, C. T. Nguyen, N. Galanis, and C. V. Popa. Experimental investigation of Al_2O_3 nanofluids thermal properties and rheology - Effects of transient and steady-state heat exposure. *International Journal of Thermal Sciences*, 76:155-167, 2014.

[10] W. Y. Lai, P. E. Phelan, and R. S. Prasher. Pressure-Drop Viscosity Measurements for γ-Al_2O_3 Nanoparticles in Water and PG-Water Mixtures (Nanofluids). *Journal of Nanoscience and Nanotechnology*, 10(12):8026-8034, 2010.

[11] S. Q. Zhou and R. Ni. Measurement of the specific heat capacity of water-based Al_2O_3 nanofluid. *Applied Physics Letters*, 92(9):2006-2009, 2008.

[12] Y. Yang, A. Oztekin, S. Neti, and S. Mohapatra. Characterization and convective heat transfer with nanofluids. *ASME/JSME 2011 8th Thermal Engineering Joint Conference, AJTEC 2011*, pages 1-6, 2011.

[13] R. L. Hamilton and O. K. Crosser. Thermal conductivity of heterogeneous two-component systems. *Industrial and Engineering Chemistry Fundamentals*, 1(3):187-191, 1962.

[14] A. Einstein. Eine neue bestimmung der molekuldimensionen. *Ann. Phys.*, 19:359-368, 1906.

[15] H. C. Brinkman. The viscosity of concentrated suspensions and solutions. *The Journal of Chemical Physics*, 20(4):571, 1952.

[16] G. K. Batchelor and J T Green. The effect of Brownian motion on the bulk stress in a suspension of spherical particles. *Journal of Fluid Mechanics*, 56(3):401-427, 1972.

[17] B.C. Pak and Y.I. Cho. Hydrodynamic and heat transfer study of dispersed fluids with submicron metallic oxide particles. *Experimental Heat Transfer*, 11(2):151-170, 1998.

[18] J. H. Lee, K. S. Hwang, S. P. Jang, B. H. Lee, J. H. Kim, S. U. S. Choi, and C. J. Choi. Effective viscosities and thermal conductivities of aqueous nanofluids containing low volume concentrations of Al_2O_3 nanoparticles. *International Journal of Heat and Mass Transfer*, 51(11-12):2651-2656, 2008.

[19] K. S. Hwang, S. P. Jang, and S. U. S. Choi. Flow and convective heat transfer characteristics of water-based Al_2O_3 nanofluids in fully developed laminar flow regime. *International Journal of Heat and Mass Transfer*, 52(1-2):193-199, 2009.

[20] K. Khanafer and K. Vafai. A critical synthesis of thermophysical characteristics of nanofluids. *International Journal of Heat and Mass Transfer*, 54(19-20):4410-4428, 2011.

[21] D. Kim, Y. Kwon, Y. Cho, C. Li, S. Cheong, Y. Hwang, J. Lee, D. Hong, and S.Moon. Convective heat transfer characteristics of nanofluids under laminar and turbulent flow conditions. *Current Applied Physics*, 9(2 SUPPL.):e119-e123, 2009.

[22] D. Wen and Y. Ding. Experimental investigation into convective heat transfer of nanofluids at the entrance region under laminar flow conditions. *International Journal of Heat and Mass Transfer*, 47(24):5181-5188, 2004.

[23] W. Williams, J. Buongiorno, and L.W. Hu. Experimental Investigation of Turbulent Convective Heat Transfer and Pressure Loss of Alumina/Water and Zirconia/Water Nanoparticle Colloids (Nanofluids) in Horizontal Tubes. *Journal of Heat Transfer*, 130(4):042412, 2008.

[24] A. R. Sajadi and M. H. Kazemi. Investigation of turbulent convective heat transfer and pressure drop of TiO_2/water nanofluid in circular tube. *Int. Commun. Heat Mass Transf.*, 38:1474-1478, 2011.

[25] R. Martínez-Cuenca, R. Mondragón, L. Hernández, C. Segarra, J.C. Jarque, T. Hibiki, and J.E. Juliá. Forced-convective heat-transfer coefficient and pressure drop of water-based nanofluids in a horizontal pipe. *Applied Thermal Engineering*, 98:841-849, 2016.

[26] S. Ferrouillat, A. Bontemps, J.P. Ribeiro, J.A. Gruss, and O. Soriano. Hydraulic and heat transfer study of SiO_2/water nanofluids in horizontal tubes with imposed wall temperature boundary conditions. *Int. J. Heat Fluid Flow*, 32(2):424-439, 2011.

[27] D. Liu and L. Yu. Single-Phase Thermal Transport of Nanofluids in a Minichannel. *Journal of Heat Transfer*, 133(3):031009, 2011.

[28] J. P. Meyer, T. J. McKrell, and K. Grote. The influence of multi-walled carbon nanotubes on single-phase heat transfer and pressure drop characteristics in the transitional flow regime of smooth tubes. *Int. J. Heat Mass Transf.*, 58:597-609, 2013.

[29] A. Nikulin, A. S. Moita, A. L. N. Moreira, S. M. S. Murshed, A. Huminic, Y. Grosu, A. Faik, J. Nieto-maestre, and O. Khliyeva. International Journal of Heat and Mass Transfer Effect of Al_2O_3 nanoparticles on laminar , transient and turbulent flow of isopropyl alcohol. *Int. J. Heat Mass Transf.*, 130:1032-1044, 2019.

[30] V. Rudyak, A. V. Minakov, D. V. Guzey, V. A. Zhigarev, and M. I. Pryazhnikov. On laminar- turbulent transition in nanofluid flows. *Thermophysics and Aeromechanics*, 23(5):773-776, 2016.

[31] W. Yu, D. M. France, E. V. Timofeeva, D. Singh, and J. L. Routbort. Thermophysical property-related comparison criteria for nanofluid heat transfer enhancement in turbulent flow. *Appl. Phys. Lett.*, 96(21), 2010.

[32] A.V. Minakov, V.Y. Rudyak, and M.I. Pryazhnikov. Rheological behavior of water and ethylene glycol based nanofluids containing oxide nanoparticles. *Colloids and Surfaces A: Physicochemical and Engineering Aspects*, 554:279-285, 2018.

[33] M. L. Huber, R. A. Perkins, A. Laesecke, D. G. Friend, J. V. Sengers, M. J. Assael, I. N. Metaxa, E. Vogel, R. Mares, and K. Miyagawa. New International Formulation for the Viscosity of H_2O. *J. Phys. Chem. Ref. Data*, 38(2), 2009.

[34] P. Leblay, J.F. Henry, D. Caron, D. Leducq, A. Bontemps, and L. Fournaison. IR thermography measurement of convective coefficients in a pipe with periodic excitation. *Int. J. Therm. Sci.*, 74:183-189, 2013.

[35] S. W. Churchill. Laminar free convection from a horizontal cylinder with a uniform heat flux density. *Letters in Heat and Mass Transfer*, 1:109-111, 1974.

[36] G.K. Filonenko. Hydraulic resistance in pipes. *Teploenergetika*, 4:40-44, 1954.

[37] M. Everts and J.P. Meyer. Flow regime maps for smooth horizontal tubes at a constant heat flux. *International Journal of Heat and Mass Transfer*, 117:1274-1290, 2018.

[38] W. M. Kays and M. E. Crawford. *Convective heat and mass transfer*. McGraw-Hill, 3rd edition, 1993.

[39] J. P. Meyer, M. Everts, N. Coetzee, K. Grote, and M. Steyn. Heat transfer coefficients of laminar, transitional, quasi-turbulent and turbulent flow in circular tubes. *International Communications in Heat and Mass Transfer*, 105:84-106, 2019.

[40] W. Y. Lai, P. E. Phelan, S. Vinod, and Ravi Prasher. Convective heat transfer for water- based alumina nanofluids in a single 1.02-mm tube. *2008 11th IEEE Intersoc. Conf. Therm. Thermomechanical Phenom. Electron. Syst. I-THERM*, 131:970-978, 2008.

[41] F. P. Incropera, D. P. Dewitt, T. L. Bergman, and A. S. Lavine. *Fundamentals of Heat and Mass Transfer*. John Wiley & Sons, 6th edition, 1993.

[42] W. Yu, D. M. France, E. V. Timofeeva, D. Singh, and J. L. Routbort. Comparative review of turbulent heat transfer of nanofluids. *International Journal of Heat and Mass Transfer*, 55(21-22):5380-5396, 2012.

[43] J. R. Taylor. *An introduction to error analysis : the study of uncertainties in physical measure- ments*. University Science Books, 1982.